HHS Public Access

Author manuscript

Nat Neurosci. Author manuscript; available in PMC 2012 June 01.

Published in final edited form as:

Nat Neurosci. ; 14(12): 1555–1561. doi:10.1038/nn.2945.

Ribbon synapses compute temporal contrast and encode luminance in retinal rod bipolar cells

Nicholas W. Oesch and **Jeffrey S. Diamond**

Synaptic Physiology Section National Institute of Neurological Disorders and Stroke National Institutes of Health Bethesda, MD 20892-3701

Abstract

Contrast is computed throughout the nervous system to encode changing inputs efficiently. The retina encodes luminance and contrast over a wide range of visual conditions and so must adapt its responses to maintain sensitivity and avoid saturation. Here we show how one type of adaptation allows individual synapses to compute contrast and encode luminance in biphasic responses to step changes in light levels. Light-evoked depletion of the readily releasable vesicle pool (RRP) at rod bipolar cell (RBC) ribbon synapses in rat retina limits the dynamic range available to encode transient but not sustained responses, thereby allowing the transient and sustained components of release to compute temporal contrast and encode mean light levels, respectively. A release/replenishment model shows that a single, homogeneous pool of synaptic vesicles is sufficient to generate this behavior and reveals that the dominant mechanism shaping the biphasic contrast/luminance response is the partial depletion of the RRP.

Introduction

Adaptation is a common computational tool used throughout the nervous system. Adaptive processes often modulate the gain of synapses, enabling them to encode inputs over a range that greatly exceeds their intrinsic output[1]. One strategy to avoid saturation is to respond selectively to changes in input (i.e., contrast), a scheme proposed to guide gain control both in the retina as well in cortical circuits[2,3]. The rod pathway in the mammalian retina adapts strongly to light stimuli, allowing it to encode both contrast and luminance across a range of background levels[1,4], but the underlying synaptic mechanisms remain poorly understood.

The gain of responses to luminance in the rod pathway is modulated over a range of background light levels via adaptation at excitatory synapses between rod bipolar cells (RBCs) and AII amacrine cells (AIIs)[5]. RBC synapses exhibit strong synaptic depression and produce biphasic (transient and sustained) responses to sustained input[6–12]. A role for synaptic depression fits well with reports that adaptation is an intrinsic feature of the RBC

Corresponding author: Jeffrey S. Diamond, Ph.D. Building 35, Room 3C-1000 35 Convent Drive Bethesda, MD 20892-3701 TEL: (301) 435-1896 FAX: (301) 435-1895 diamondj@ninds.nih.gov.

Author Contributions N.W.O. and J.S.D. conceived the project and designed the experiments; N.W.O. performed the experiments and analyzed the data; N.W.O. designed the mathematical model; N.W.O. and J.S.D. wrote the manuscript.

presynaptic terminal[5,13], but the specific depression mechanism underlying luminance adaptation has not been identified. At the RBC synapse, depletion of the RRP is thought to underlie biphasic responses[7,8,14,15] and has been argued to be a mechanism of gain modulation[13,16], but it is unclear whether these two phenomena are mechanistically related. Furthermore, a clear computational role for gain modulation has yet to be demonstrated at this synapse.

To examine how the transient and sustained components of RBC signaling relay visual information, we compared light-evoked responses in RBCs and AII amacrine cells. We found that synaptic release from RBC ribbon synapses adapts to step increases in luminance, thereby generating a transient component in the AII response that encodes contrast over a range of background light levels. In addition, the sustained component of the AII response faithfully represents the RBC response and provides a reliable measure of luminance regardless of stimulus history. To identify the synaptic mechanisms underlying this adaptation, we recorded from synaptically coupled RBC-AII pairs and evoked EPSCs in the AII with voltage steps in the RBC. We found that rapid, partial depletion of the RRP underlies the transient component of the AII excitatory postsynaptic current (EPSC) and adaptation to increased stimuli; subsequent release from and replenishment to the partially depleted RRP produces a sustained release rate that encodes the RBC luminance signal. A simple model indicates that depletion and replenishment of a kinetically homogeneous vesicle pool accounts for this behavior. These results show how tight regulation of RRP occupancy enables RBC ribbon synapses to parse visual information into multiple streams.

Results

Dual-component responses encode luminance and contrast

Previous work suggests that the RBC-AII synapse is a key locus of adaptation in the rod pathway[5,13]. To examine adaptation at this glutamatergic synapse, we measured (in separate experiments) light-evoked voltage responses from the RBC and EPSCs in the AII (Fig. 1). Inhibition was blocked (see methods) to facilitate comparison with subsequent paired RBC-AII recordings (described below). The light stimulus comprised a full-field, 2–3-s step from darkness to a range of "background" levels (φ_b = 0.14 –7.12 r* per rod per s), followed by a 2-s step to a greater "test" intensity (φ_t). φ_t varied with φ_b so that the Weber contrast between the two steps (($\varphi_t - \varphi_b$) / φ_b) varied roughly five-fold over the range of φ_b.

We made perforated-patch current-clamp recordings from RBCs to measure light-evoked changes in RBC membrane potential (V_{RBC}). Light steps from darkness to different φ_b levels evoked depolarization from rest (V_{rest} = −50.3 ± 2.5 mV; n = 5) that increased with φ_b (Fig. 1a,c,e). Light-evoked depolarization persisted for the duration of the light step, consistent with previously reported whole-cell voltage responses[17] and voltage-clamped current recordings in which intracellular calcium buffering approximated endogenous levels[9,18]. V_{RBC} values following steps from φ_b to φ_t were not different than those following steps from darkness to the same intensity (Fig. 1e), indicating that V_{RBC} encodes absolute light levels but not contrast. For φ values below 7 r* per rod per s, V_{RBC} followed a function of light intensity ($V_{RBC}(\varphi)$) that was well fit by the Hill equation and was similar in shape (if not sensitivity) to that of photoreceptors[19–21]. For log-linear intensity-response functions,

changes in response are proportional to Weber contrast[22–24], and a similar relationship exists over the middle range of the Hill function[4] (see supplementary equations and supplementary Fig. 1). Accordingly, the arithmetic difference between $V_{RBC}(\varphi_t)$ and $V_{RBC}(\varphi_b)$ corresponded to the Weber contrast between φ_t and φ_b (Fig. 1g). The observation that V_{RBC} does not adapt over this stimulus range is consistent with previous work showing that adaptation near visual threshold occurs downstream of the V_{RBC} signal[5].

To determine how adaptation at the RBC ribbon synapses shapes the visual information conveyed to the AII, we made whole-cell voltage-clamp recordings from postsynaptic AIIs and elicited EPSCs with the same light stimulation protocol described above. AII EPSCs are not shaped significantly by postsynaptic receptor saturation or desensitization and so accurately reflect release from RBCs[14,25]. Light-evoked EPSCs in AIIs comprised transient and sustained components (Fig. 1b,d; see also[26,27]). The sustained component, measured during the last 0.5 s of either light step (see methods), varied with the absolute intensity of the step regardless of the preceding background intensity (Fig. 1f), much like V_{RBC} (Fig. 1e). Interestingly, the charge transfer of the transient component (see methods) of the AII EPSC elicited by steps from φ_b to φ_t reliably reported the Weber contrast between φ_b and φ_t (Fig. 1h; r^2 of mean = 0.847, $p<0.001$; n=10 cells). These results were obtained at room temperature (22°C); in other experiments at 35°C with inhibition intact, the transient and sustained components of the AII EPSC also encoded measures of contrast and luminance (supplementary Fig. 2).

Contrast is computed by RBC ribbon synapses

Contrast signals in AII EPSCs may reflect processing throughout the retinal circuitry[28] and/or within the RBCs ribbon synapses. To distinguish these possibilities, we functionally isolated RBC synapses with simultaneous whole-cell voltage-clamp recordings from synaptically coupled RBCs and AIIs (Fig. 2). EPSCs were evoked in the postsynaptic AIIs with depolarizing steps delivered to the presynaptic RBC. Inhibition was blocked, and spontaneous release from ON bipolar cells was reduced with the group III mGluR agonist L-AP4 (10 μM)[25]. To approximate the light experiments described above, V_{RBC} was stepped to a range of "background" potentials (V_b = −50 mV to −30 mV) for 1 s, followed by a 1-s step to a "test" potential ($V_t = V_b + 10$ mV). Although RBC Ca_v currents were relatively sustained during the first voltage step, AII EPSCs exhibited transient components across the entire range of V_b (Fig. 2a), similar to light-evoked EPSCs (Fig. 1e–f). This result is consistent with previous reports that biphasic release from RBCs cannot be accounted for by presynaptic Ca_v channel inactivation or feedback inhibition[10]. During the first step (to V_b), the amplitude of the transient component and the frequency of synaptic events during the sustained component varied over the range of V_b and closely followed the amplitude of the Ca_v current (Fig. 2b,c; see also[10,29,30]). In striking analogy to the light-evoked EPSCs, the sustained component of the response to V_t reliably followed the magnitude of presynaptic depolarization independently of the stimulus history (Fig. 2b). Moreover, the transient component reliably encoded the difference in the sustained response to V_t and V_b (Fig. 2c), analogous to the observation that the transient component of light-evoked EPSCs encoded Weber contrast between φ values (Fig. 1h).

RRP occupancy encodes luminance and helps compute contrast

Depletion of the RRP has been proposed as a primary mechanism of synaptic depression at RBC synapses. Based on previous work[7,8,14], we had expected the transient component of the EPSC to reflect the complete depletion of the RRP, thereby strongly limiting subsequent responses (but see [12,31]). The data presented here (Fig. 2) suggest, however, that even partial RRP depletion is sufficient to generate a transient response. For example, a voltage step to V_b= −40 mV evoked a dual-component EPSC (middle AII EPSC, Fig. 2a), and a subsequent step to V_t = −30 mV elicited another transient response, indicating that the RRP was at least partially occupied during the sustained response to V_b. To explore this idea further, we measured the size of the RRP at different "background" potentials (Fig. 3). In paired RBC-AII recordings, a 1-s voltage step in the RBC to a range of V_b levels (−55 to −25 mV) was followed by a 1-s step to V_t = −20 mV. Previous work has shown that a step to −20 mV completely depletes the RRP and that miniature EPSCs sum linearly so that the charge transfer of the transient component of the EPSC ($Q_{transient}$) reflects the size of the available RRP[14]. Accordingly, steps from V_b = −25 mV to V_t = −20 mV elicited no detectable transient EPSC, indicating effective depletion of the RRP at −25 mV (Fig. 3a). Voltage steps to V_t from intermediate V_b levels elicited transient responses with a range of $Q_{transient}$ values that varied with V_b (Fig. 3a,b), indicating that the occupancy of the RRP varies continuously between nearly full and almost empty across the V_{RBC} range subtended in response to light stimulation (−50 mV to −25 mV; Fig. 1c).

Integrating release over time demonstrated that the rate of release after the transient response remained nearly constant for the duration of the step (Fig. 3c). To test whether RRP occupancy remains constant during sustained release, we measured the size of the RRP at different times during sustained release at an intermediate potential. In paired RBC-AII recordings, the RBC was stepped from −70 mV to −40 mV, followed by a step to −20 mV at varying intervals (0.05 to 2 seconds). Prior to recording each time series, the RBC was stepped from −70 mV directly to −20 mV to obtain the size of the entire RRP (black traces, Fig. 4). Stepping the RBC to −40 elicited a transient response corresponding to approximately half the full RRP (Fig. 4b). The subsequent step to −20 mV evoked a transient response corresponding to the remaining 50% of the RRP, regardless of the interval between the two steps (Fig. 4b,c), indicating that RRP occupancy remains constant during sustained depolarization.

The fact that release rate and RRP occupancy remain constant during sustained release indicates that the release rate reflects a steady-state equilibrium between vesicle release and replenishment. Therefore, V_{RBC} is reflected not only in the sustained rate of release, to encode luminance, but also in the steady-state occupancy of the RRP. Because $Q_{transient}$ is equal to the number of vesicles released during a change in steady-state RRP occupancy, which is determined by V_{RBC}, and because differences in V_{RBC} approximate Weber contrast (Fig. 1d), we conclude that depletion of the RRP represents the mechanism by which contrast is encoded by the RBC ribbon synapse.

Our results suggest that the steady-state occupancy of the RRP should decrease as the background light level (φ_b) increases. To test this prediction, we presented a full field, 2–3 second step from darkness to a range of background light levels (φ_b = 0.14 −10.3 r* per rod

per s) followed by a 2 second step to a high, fixed test intensity (φ_t = 13.69 r* per rod per s; Fig. 5). Perforated-patch and whole-cell recordings were made (in separate experiments) from RBCs (Fig. 5a,c,e) and AIIs (Fig. 5b,d,f), respectively. Steps to φ_b elicited a range of depolarizations in RBCs; V_{RBC} in response to φ_t reached the same maximal level independently of V_b (Fig. 5e). The transient component of the AII EPSC elicited by φ_t was smaller with increasing φ_b, such that the sum of the transient responses to φ_b and φ_t was constant over the entire range (Fig. 5f), analogous to results from paired recordings (Fig. 3b). While the transient response reliably encoded $V_{RBC}(\varphi_t)$-$V_{RBC}(\varphi_b)$ (Fig. 5f), this difference did not correspond to Weber contrast because here φ_t exceeded the RBC response range (Fig. 1e).

Contrast can be computed by one homogenous vesicle pool

Our experimental results indicate that different phases of release from RBC synapses encode different features of the visual world. Release at other central synapses also exhibits multiple components (see[32]), perhaps because vesicles express multiple isoforms of molecules (e.g., synaptotagmin) that contribute to release with different kinetics[33,34], or because vesicles experience different calcium signals[35,36]. Some mechanisms causing release heterogeneity have been shown to operate at ribbon synapses [9,31]. To examine whether the biphasic release observed here requires multiple, kinetically distinct vesicle pools within the RRP, we constructed a simple release model (Fig. 6). At V_{RBC} = −70 mV, a 55 release site RRP^{14} was occupied by a homogeneous pool of vesicles with identical release characteristics. Vesicle release probability varied with V_{RBC} according to measured values of release rate and pool size (see methods). Following release, vacant release sites (also identical) were refilled with a probability that varied with V_{RBC} so that steady state RRP occupancy matched our experimental results (Fig. 3b; see methods). Vesicle release and replenishment during a time step (0.1 ms) was determined randomly for each site according to the release and replenishment probability determined by V_{RBC}. To simulate EPSC recordings, each release event was represented by a characteristic mEPSC waveform that was added at the appropriate time to the simulated EPSC (see methods).

When driven by the V_{RBC} waveforms used in the paired recording experiments, the model produced EPSCs that reproduced several key features of the experimental data (Fig. 6a,b). Specifically: release was transient for sub-maximal voltage steps; both release components increased over a range of presynaptic voltages (Fig. 6d,e); the sustained release rate did not depend on stimulus history (Fig. 6d), making it a reliable readout of V_{RBC}; the transient response to a fixed step reliably encoded the difference between the sustained response to V_t and V_b (Fig. 6e); and the transient response to a fixed V_t step decreased with increasing V_b (Fig. 6b,g). Changes in RRP occupancy occurred during the transient component of the EPSC; $Q_{transient}$ reflected the difference in steady-state occupancy levels and sustained release corresponded to a non-zero steady state level of RRP occupancy (Fig. 6c,f).

In the model (and in the paired recordings), transient responses were particularly apparent because abrupt changes in V_{RBC} elicited rapid increases in release probability and high release rates before RRP occupancy reached steady-state at new, lower levels. To test whether slower, light-evoked signals in RBCs also generate transient and sustained release

in simulated AII EPSCs, we drove the model with the light-evoked voltage waveforms recorded in RBCs (Figs. 1 and 7). Here, the model again reproduced key features of the experimental data (Fig. 7). In particular, the simulated sustained component encoded luminance (Fig. 7c) and the transient response reliably reported the Weber contrast between φ_b and φ_t (Fig. 7d). While these results do not preclude the existence of multiple vesicle pools, the model achieved biphasic release and contrast computation with a single, homogeneous RRP.

Discussion

Here we report that RBC ribbon synapses respond to increased luminance with two phases of release, each encoding a distinct feature of the stimulus. The transient component, reflecting the rapid, partial depletion of the RRP, encodes Weber contrast between two light levels; the sustained component, reflecting steady-state release from a partially filled RRP, encodes absolute luminance. Recordings between synaptically coupled RBC-AII cell pairs confirmed that contrast is computed intrinsically by RBC synapses. Specifically, the steady-state release rate *and* RRP occupancy represent log-linear functions of luminance; contrast is encoded in the transient response that occurs when the RRP occupancy decreases in response to increased luminance. The quantal content of the transient response reflects the reduction in the available RRP between the two luminance levels; due to the log-linear relationship between RRP occupancy and luminance (Fig. 5f), this difference corresponds to Weber contrast (supplementary equations). A simple release model suggested that such biphasic signaling may be achieved with a single, homogeneous vesicle pool. This work establishes RRP depletion as a synaptic mechanism of adaptation that enables RBC ribbon synapses to compute Weber contrast, and transmit multiple types of visual information.

Adaptation in visual signaling

The most salient features in our visual world are best represented by contrast[37]. Accordingly, contrast signals originate in the retina and are utilized throughout the visual pathway[2]. Calculating contrast requires neural adaptation to background luminance[2], but, although the properties of visual adaptation have been well-studied, the specific synaptic mechanisms that compute contrast in the retina had not been identified[1,4].

Both psychophysics and in vitro physiology have demonstrated that luminance adaptation occurs in the inner retina[2,4]. Luminance adaptation in the rod pathway occurs at the synapse between the RBC and AII[5], and synapse-specific depression occurs presynaptic to the AII in responses at the visual threshold[13]. Taken together, these studies suggest that luminance adaptation occurs through a mechanism of synaptic depression intrinsic to the RBC ribbon synapse. Our results confirm this hypothesis, identify the synaptic mechanism underlying this adaptation, and show that it computes the value of Weber contrast in the stimulus. Our results do not exclude roles for other types of adaptation in the inner retina[2]. A slow component in the light-evoked AII EPSC (figures 1,5), not evident in the paired recordings (Figs. 2 and 3) may reflect a slow adaptation mechanism previously described[38].

Vesicle release and replenishment at RBC ribbon synapses

RBC ribbon synapses encode luminance and contrast in two, kinetically distinct phases of release (Fig. 1). Biphasic release in response to constant input has been observed in RBCs[6–10,12] and elsewhere[15,32,39–43] and is often thought to reflect a kinetically diverse RRP. Kinetic heterogeneity may be attributed to different calcium sensors in the vesicle membrane[33,34,44], or release kinetics of otherwise identical vesicles may vary with their position relative to calcium channels[9,31,35,36,45,46].

Our results demonstrate that transient release, and RRP occupancy, is graded over a range of V_{RBC}. This allows the transient component of release to vary according to the difference in V_{RBC}, a computation that would not be possible if the dynamic range of RRP occupancy were not matched to the physiological range of V_{RBC}. Our model demonstrated that, for experimentally observed release and replenishment rates, a single kinetically homogeneous RRP can achieve biphasic release and maintain partial steady-state RRP occupancy during sustained responses. A similar model and interpretation has been proposed to account for synchronous and asynchronous release in the cochlear nucleus with a single, homogeneous RRP[40]. Experimental evidence suggests that vesicles in RBC terminals experience a range of calcium signals[9,31], so our model likely oversimplifies RRP dynamics. Heterogeneous release characteristics are not required to generate transient and sustained release at this synapse (Fig. 6), and specific roles for this additional complexity remain unknown.

Experimental work suggests that the rate of vesicle replenishment at many synapses may depend on presynaptic calcium (reviewed by[47]). To model vesicle release and replenishment at different V_{RBC} values, we estimated release and replenishment probabilities during steady-state release (see methods); the replenishment probability at each empty release site was essentially constant across the physiological range of V_{RBC} (supplementary Fig. 3). While the overall replenishment rate clearly varies with V_{RBC}, in our model this reflected changes in the number of empty release sites and did not require replenishment probability to be calcium-dependent.

AIIs may parse visual information to distinct targets

RBC synapses may encode luminance and contrast to enable AIIs to transmit distinct visual information to different postsynaptic targets. For example, the AII may convey sustained luminance information through its electrical synapses to ON cone bipolar cells, thereby relaying the RBC signal to its cone pathway counterpart. In this scenario, the ON cone bipolar cell, which normally receives photopic luminance information from cones, could make the same contrast calculation at night that it does during the day. At the same time, the AII may relay the transient signal through inhibitory, glycinergic synapses to OFF ganglion cells that encode contrast. AIIs also contact OFF cone bipolar cells via glycinergic synapses and may tailor these outputs to the specific needs of different OFF cone bipolar cell subtypes. Na_v conductances, which accelerate the rising phase of AII depolarizations[48], may help direct luminance and contrast signals to their appropriate targets.

Methods

Slice and Recording Procedures

All animal procedures were conducted in accordance with NIH guidelines, as approved by the National Institute of Neurological Disorders and Stroke Animal Care and Use Committee. Acute slices (200 μm thick) were prepared from retina isolated from Sprague-Dawley rats (p18–p22) as previously described[10]. Retinas were isolated and all subsequent procedures and recordings were performed in Ames media equilibrated with 95% O_2/5% CO_2. For light response experiments, rats were dark-adapted for 2–3 hours and dissection and all subsequent procedures were performed in darkness or under IR illumination (840 nm). For paired recording experiments animals were housed and dissected under ambient laboratory lighting. To ensure that differences light adaptation state would not confound the comparison between paired recordings and light-evoked responses, we performed a subset of paired recording experiments in retinal slices that were dark-adapted as in the light response experiments. No difference was observed between the two conditions (supplementary Fig. 4) and so both paired recordings from both light and dark adapted pairs were pooled (Fig. 2). In all experiments sodium channels and inhibitory transmission was blocked during recording with the addition of 0.5 μM TTX (Ascent Scientific), 10 μM SR-95531 (Ascent Scientific), 3 μM strychnine (Sigma), and 50 μM TPMPA (Tocris) to the recording solution. For paired recording experiments the mGluR6 selective agonist (L-AP4 10 μm; Tocris) was added to the recording solution to simulate darkness (i.e, sustained glutamate release from rods) and hyperpolarize RBCs. RBCs and AIIs were targeted visually using IR (840 nM) DIC video microscopy. Whole-cell voltage-clamp and perforated patch current-clamp recordings were made with pipettes (4–6 MΩ) filled with solution containing (in mM) 90 $CsCH_3SO_4$, 20 TEA-Cl, 10 HEPES, 10 EGTA, 10 phosphocreatine disodium salt hydrate, 4 Mg-ATP, 0.4 Na-GTP. For perforated-patch current-clamp recordings, KCH_3SO_4 was substituted for $CsCH_3SO_4$ and ~1.0 mg/ml solubilized Amphotericine B (sigma) was added to the recording solution. Pipette tips were filled with Amphotericine-free solution. Recordings were obtained using an axopatch 700B amplifier (Molecular Devices), low-pass filtered at 4 kHZ (Bessel) and digitized at 20–50 kHz with an Instrutech ITC-18 A/D board (HEKA Elektronik) controlled by custom acquisition software written in IgorPro (WaveMetrics). Some traces were down-sampled or down-sampled and filtered for display. Data was digitally filtered using a binomial smoothing algorithm (IgorPro) to approximate a Gaussian filter with a characteristic cutoff frequency (denoted in the figure legends).

Light Stimulation

Light stimuli were generated with a 528-nm LED and directed through a 1.0 NA 40 X water-immersion objective (Zeiss) to uniformly illuminate the 0.45 mm-diameter field of view. LED intensity was attenuated with neutral density filters and further controlled by pulse width modulation of the LED (10 ms duty cycle) using a custom-built constant current power supply controlled through the ITC-18 by the acquisition software. Photon flux was measured at the focal plane of the microscope objective using a DR-2000 radiometer (Gamma Scientific) and was converted to photoisomerizations (r*)/rod assuming a collecting area of 0.5 μm[49]. In both light stimulation and paired recording experiments,

stimuli were presented at 15 second intervals. Except where noted, all experiments were performed at room temperature (~22°C).

Data Analysis

To measure sustained release during light responses, we averaged the current response over the last 0.5 seconds of the light step relative to the baseline preceding the first light-step. For paired recordings we measured the rate of sustained EPSCS by identifying individual EPSC events using custom miniature analysis over the last 0.9 seconds of the voltage step. This yielded similar results to measuring average current amplitude or integrated current over the same time window. To examine transient release components for either light-evoked or paired recordings, we integrated release over the transient component and corrected for the baseline immediately preceding the transient response. For comparison all we have normalized all transient and sustained responses to the maximal response.

Computer simulations

To model synaptic release at the RBC we generated a Monte Carlo type computer simulation where vesicles were randomly released or replenished to a "RRP" according to release and replenishment probabilities we measured from our data. We first estimated the size of the RRP in our paired recording experiments by measuring the charge transfer of the transient response to a voltage step from −70 mV to −20 mV. Dividing the charge transfer of the EPSC by that of the average miniature EPSC waveform yielded an average full RRP value of approximately 55 vesicles, in close agreement with previous estimates[10,25]. Multiplying the total RRP size by the measured fractional RRP occupancy (Fig. 3) allowed us to generate a function relating the number of vesicles or empty sites in the RRP to V_{RBC}. To obtain release and replenishment rates for V_{RBC}, we reasoned that if the RRP size does not change then release and replenishment rate must be at a steady-state equilibrium so and the rates of release and replenishment must be equal. We measured rate of vesicle release from the EPSC count as well as the slope of the integrated release during steady-state release; both measurements yielded similar results. To obtain the release probability we divided the release-rate at V_{RBC} by the number of vesicles in the pool at V_{RBC}. Similarly, we divided the replenishment rate by the number of empty release sites (RRP_{total}-$RRP_{occupancy}$) to obtain the probability of replenishment. We then fit the data points with Hill equations from −70 to 0 mV, to interpolate V_{RBC} between our data points. Because past work has shown that the rate of replenishment is very low when the RBC is held at hyperpolarized potentials[14], we constrained the base of the Hill fit at −70 V_{RBC} to fit with this observation (supplementary Fig. 3). Responses were simulated over discrete time steps (0.1 ms). At each time point, the release or replenishment of each release site was determined individually by comparing a number from a random number generator to the release and replenishment probabilities at $V_{RBC}(t)$. If a vesicle was to be released, a characteristic mEPSC waveform was added to the current trace at that time step; the number of vesicles and empty sites in the RRP was updated at the end of each time step.

Supplementary Material

Refer to Web version on PubMed Central for supplementary material.

Acknowledgements

We thank Gabe Murphy for helpful discussions and W. Wade Kothmann, Alon Poleg-Polsky and Annalisa Scimemi for comments on the manuscript. This work was supported by the NINDS Intramural Research Program.

References

1. Rieke F, Rudd ME. The challenges natural images pose for visual adaptation. Neuron. 2009; 64:605–616. [PubMed: 20005818]
2. Shapley R, Enroth-Cugell C. Visual adaptation and retinal gain controls. Prog Retinal Res. 1984; 3:263–346.
3. Abbott LF, Varela JA, Sen K, Nelson SB. Synaptic depression and cortical gain control. Science. 1997; 275:220–224. [PubMed: 8985017]
4. Green DG. The search for the site of visual adaptation. Vision Res. 1986; 26:1417–1429. [PubMed: 3303666]
5. Dunn FA, Doan T, Sampath AP, Rieke F. Controlling the gain of rod-mediated signals in the Mammalian retina. J Neurosci. 2006; 26:3959–3970. [PubMed: 16611812]
6. von Gersdorff H, Matthews G. Dynamics of synaptic vesicle fusion and membrane retrieval in synaptic terminals. Nature. 1994; 367:735–739. [PubMed: 7906397]
7. Mennerick S, Matthews G. Ultrafast exocytosis elicited by calcium current in synaptic terminals of retinal bipolar neurons. Neuron. 1996; 17:1241–1249. [PubMed: 8982170]
8. von Gersdorff H, Matthews G. Depletion and replenishment of vesicle pools at a ribbon-type synaptic terminal. J. Neurosci. 1997; 17:1919–1927. [PubMed: 9045721]
9. Burrone J, Neves G, Gomis A, Cooke A, Lagnado L. Endogenous calcium buffers regulate fast exocytosis in the synaptic terminal of retinal bipolar cells. Neuron. 2002; 33:101–112. [PubMed: 11779483]
10. Singer JH, Diamond JS. Sustained Ca2+ entry elicits transient postsynaptic currents at a retinal ribbon synapse. J. Neurosci. 2003; 23:10923–10933. [PubMed: 14645488]
11. Trexler EB, Li W, Massey SC. Simultaneous contribution of two rod pathways to AII amacrine and cone bipolar cell light responses. J. Neurophysiol. 2005; 93:1476–1485. [PubMed: 15525810]
12. Snellman J, Zenisek D, Nawy S. Switching between transient and sustained signalling at the rod bipolar-AII amacrine cell synapse of the mouse retina. J. Physiol. (Lond.). 2009; 587:2443–2455. [PubMed: 19332496]
13. Dunn FA, Rieke F. Single-photon absorptions evoke synaptic depression in the retina to extend the operational range of rod vision. Neuron. 2008; 57:894–904. [PubMed: 18367090]
14. Singer JH, Diamond JS. Vesicle depletion and synaptic depression at a mammalian ribbon synapse. J. Neurophysiol. 2006; 95:3191–3198. [PubMed: 16452253]
15. Jackman SL, et al. Role of the synaptic ribbon in transmitting the cone light response. Nat Neurosci. 2009; 12:303–310. [PubMed: 19219039]
16. Jarsky T, et al. A synaptic mechanism for retinal adaptation to luminance and contrast. J. Neurosci. 2011; 31:11003–11015. [PubMed: 21795549]
17. Euler T, Masland RH. Light-evoked responses of bipolar cells in a mammalian retina. J. Neurophysiol. 2000; 83:1817–1829. [PubMed: 10758094]
18. Berntson A, Smith RG, Taylor WR. Postsynaptic calcium feedback between rods and rod bipolar cells in the mouse retina. Vis. Neurosci. 2004; 21:913–924. [PubMed: 15733346]
19. Naka KI, Rushton WA. S-potentials from luminosity units in the retina of fish (Cyprinidae). J. Physiol. (Lond.). 1966; 185:587–599. [PubMed: 5918060]
20. Baylor DA, Fuortes MG. Electrical responses of single cones in the retina of the turtle. J. Physiol. (Lond.). 1970; 207:77–92. [PubMed: 4100807]
21. Baylor DA, Nunn BJ, Schnapf JL. The photocurrent, noise and spectral sensitivity of rods of the monkey Macaca fascicularis. J. Physiol. (Lond.). 1984; 357:575–607. [PubMed: 6512705]
22. Boynton RM, Whitten DN. Visual adaptation in monkey cones: recordings of late receptor potentials. Science. 1970; 170:1423–1426. [PubMed: 4991522]

23. Normann RA, Werblin FS. Control of retinal sensitivity. I. Light and dark adaptation of vertebrate rods and cones. J Gen Physiol. 1974; 63:37–61. [PubMed: 4359063]
24. Werner G, Mountcastle VB. Neural activity in mechanoreceptive cutaneous afferents: Stimulus-response relations, Weber functions, and information transmission. J. Neurophysiol. 1965; 28:359–397. [PubMed: 14283062]
25. Singer JH, Lassová L, Vardi N, Diamond JS. Coordinated multivesicular release at a mammalian ribbon synapse. Nat. Neurosci. 2004; 7:826–833. [PubMed: 15235608]
26. Pang JJ, Gao F, Wu SM. Light-evoked current responses in rod bipolar cells, cone depolarizing bipolar cells and AII amacrine cells in dark-adapted mouse retina. J. Physiol. (Lond.). 2004; 558:897–912. [PubMed: 15181169]
27. Xin D, Bloomfield SA. Comparison of the responses of AII amacrine cells in the dark- and light-adapted rabbit retina. Vis Neurosci. 1999; 16:653–665. [PubMed: 10431914]
28. DeVries SH, Baylor DA. An alternative pathway for signal flow from rod photoreceptors to ganglion cells in mammalian retina. Proc. Natl. Acad. Sci. U.S.A. 1995; 92:10658–10662. [PubMed: 7479860]
29. Keen EC, Hudspeth AJ. Transfer characteristics of the hair cell's afferent synapse. Proc. Natl. Acad. Sci. U.S.A. 2006; 103:5537–5542. [PubMed: 16567618]
30. Jarsky T, Tian M, Singer JH. Nanodomain control of exocytosis is responsible for the signaling capability of a retinal ribbon synapse. J. Neurosci. 2010; 30:11885–11895. [PubMed: 20826653]
31. Beaumont V, Llobet A, Lagnado L. Expansion of calcium microdomains regulates fast exocytosis at a ribbon synapse. Proc. Natl. Acad. Sci. U.S.A. 2005; 102:10700–10705. [PubMed: 16027365]
32. Goda Y, Stevens CF. Two components of transmitter release at a central synapse. Proc Natl Acad Sci USA. 1994; 91:12942–12946. [PubMed: 7809151]
33. Geppert M, et al. Synaptotagmin I: a major Ca2+ sensor for transmitter release at a central synapse. Cell. 1994; 79:717–727. [PubMed: 7954835]
34. Sun J, et al. A dual-Ca2+-sensor model for neurotransmitter release in a central synapse. Nature. 2007; 450:676–682. [PubMed: 18046404]
35. Sakaba T, Neher E. Quantitative relationship between transmitter release and calcium current at the calyx of held synapse. J. Neurosci. 2001; 21:462–476. [PubMed: 11160426]
36. Wadel K, Neher E, Sakaba T. The coupling between synaptic vesicles and Ca2+ channels determines fast neurotransmitter release. Neuron. 2007; 53:563–575. [PubMed: 17296557]
37. Land EH, McCann JJ. J Opt Soc Am. 1971; Vol. 61:1–11. [PubMed: 5541571]
38. Adelson EH. Saturation and adaptation in the rod system. Vision Res. 1982; 22:1299–1312. [PubMed: 7179751]
39. Atluri PP, Regehr WG. Delayed release of neurotransmitter from cerebellar granule cells. J. Neurosci. 1998; 18:8214–8227. [PubMed: 9763467]
40. Lu T, Trussell LO. Inhibitory transmission mediated by asynchronous transmitter release. Neuron. 2000; 26:683–694. [PubMed: 10896163]
41. Otsu Y, et al. Competition between phasic and asynchronous release for recovered synaptic vesicles at developing hippocampal autaptic synapses. J. Neurosci. 2004; 24:420–433. [PubMed: 14724240]
42. Hefft S, Jonas P. Asynchronous GABA release generates long-lasting inhibition at a hippocampal interneuron-principal neuron synapse. Nat. Neurosci. 2005; 8:1319–1328. [PubMed: 16158066]
43. Peters JH, Mcdougall SJ, Fawley JA, Smith SM, Andresen MC. Primary afferent activation of thermosensitive TRPV1 triggers asynchronous glutamate release at central neurons. Neuron. 2010; 65:657–669. [PubMed: 20223201]
44. Pang ZP, Südhof TC. Cell biology of Ca2+-triggered exocytosis. Current Opinion in Cell Biology. 2010; 22:496–505. [PubMed: 20561775]
45. Quastel DM, Guan YY, Saint DA. The relation between transmitter release and Ca2+ entry at the mouse motor nerve terminal: role of stochastic factors causing heterogeneity. Neuroscience. 1992; 51:657–671. [PubMed: 1362600]
46. Borst JG, Sakmann B. Calcium influx and transmitter release in a fast CNS synapse. Nature. 1996; 383:431–434. [PubMed: 8837774]

47. Neher E, Sakaba T. Multiple roles of calcium ions in the regulation of neurotransmitter release. Neuron. 2008; 59:861–872. [PubMed: 18817727]

48. Tian M, Jarsky T, Murphy GJ, Rieke F, Singer JH. Voltage-gated Na channels in AII amacrine cells accelerate scotopic light responses mediated by the rod bipolar cell pathway. J. Neurosci. 2010; 30:4650–4659. [PubMed: 20357115]

49. Field GD, Rieke F. Nonlinear signal transfer from mouse rods to bipolar cells and implications for visual sensitivity. Neuron. 2002; 34:773–785. [PubMed: 12062023]

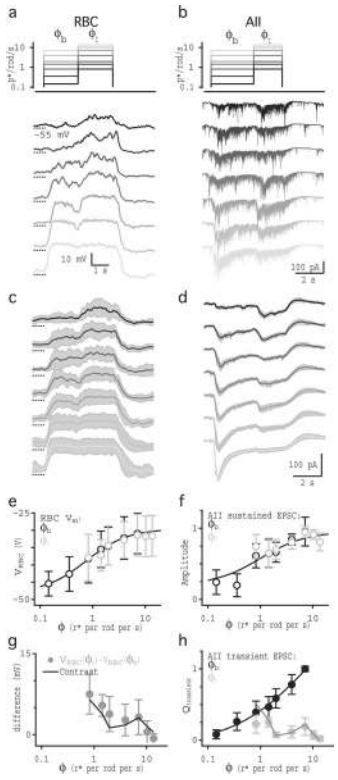

Fig. 1.

RBC synaptic release encodes both contrast and luminance. (a) Perforated-patch current-clamp recordings from a single RBC show voltage responses to steps in φ for full-field light stimulation. The schematic shows the light intensity of the step to φ_b and to φ_t. The grayscale of the schematic trace corresponds to the grayscale in the response traces below. (b) Whole-cell voltage-clamp recordings from a single AII in response to the same light stimulation protocol used in (a). (c) Average ± SD (gray shading) light-evoked voltage responses in 5 RBCs. Traces were down-sampled to 1kHz resolution before averaging. (d) Average (± SD, gray shading) light-evoked EPSCs in 10 AIIs. Traces were down sampled to 0.1 kHz and smoothed with a 12 Hz cutoff Gaussian filter before averaging. (e) Average responses in RBCs (± SD; n = 5 cells) to φ_b (black) and φ_t (gray) plotted against φ. (f) Average current responses in AIIs (± SD; n = 10 cells) measured over the last 0.1 s of φ_b (black) and φ_t (gray), plotted against φ. (g) Subtraction of $V_b(\varphi_b)$ from $V_t(\varphi_t)$ in RBCs plotted against φ_t (light gray). The contrast between φ_b and φ_t, scaled to match the subtraction, is shown for comparison (black). (h) Integrated current (average ± SD; n = 10 cells) measured over the transient component of AII responses to φ_b (black) and φ_t (light gray), plotted against φ. Gray line shows the contrast step size between φ_b and φ_t plotted against φ_t, scaled to match $Q(\varphi_t)$. Solid dark gray lines in e, f and h are Hill equation fits to the data.

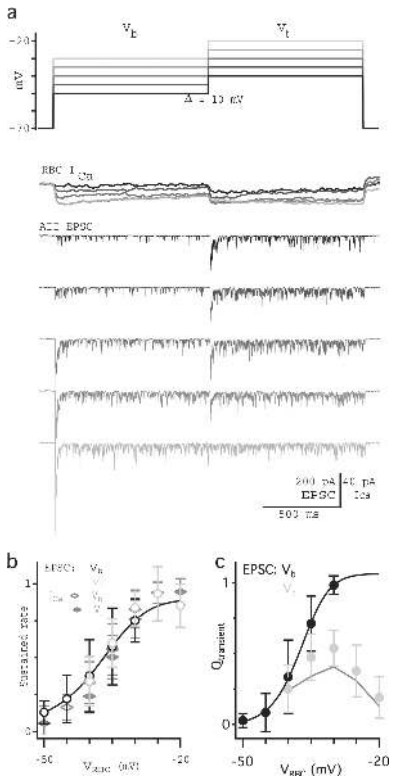

Fig. 2.

Contrast is computed at the RBC synapse. (a) Individual current recordings from synaptically coupled RBC-AII pairs show typical RBC Ca_v currents and AII EPSCs, evoked by stepping V_{RBC} to a background potential (V_b) for 1 s followed by a 1 s test step (V_t) that was 10 mV more depolarized than the background step. The grayscale of the schematic trace corresponds to the grayscale in the response traces below. Calcium currents in the RBC were measured using a p/4 subtraction protocol, down-sampled to 1kHz resolution and filtered using a 60 Hz cutoff Gaussian filter. (b) Rate (average ± SD) of EPSCs measured over the last 0.5 s of the step for V_b (black) and V_t (light gray). (c) Integrated current (average ± SD; n = 15 cells) measured over the transient component of the response to V_b (black) and V_t (light gray), plotted against V_{RBC}. Dark gray line shows the subtraction between the rate(V_t) and rate(V_b). Solid black lines in b and c are the Hill equation fits to the data.

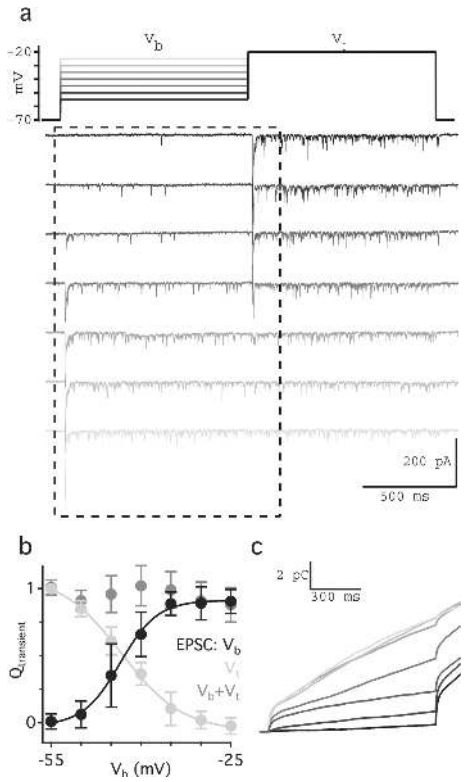

Fig. 3.

RRP continuously varies with V_{RBC}. (a) Individual current recordings show typical AII EPSCs evoked by stepping V_{RBC} to a background potential for 1 s followed by a 1 s test step to −20 mV. (b) Average integrated current (± SD; n = 10 cells) measured over the transient component of the response to V_b (black) and V_t (light gray), plotted against φ_t. The arithmetic sums of the transient responses to V_b and V_t are plotted in dark gray. (c) Integrated current traces corresponding to the current traces shown in panel a during V_b and a portion of V_t.

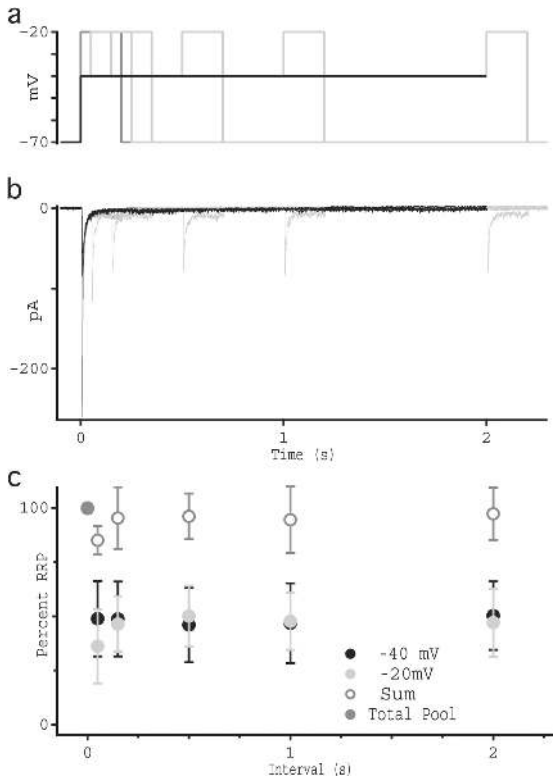

Fig. 4.

RRP occupancy is constant during sustained release. (a) Voltage protocol used to measure RRP occupancy over time. Step from −70 to −20 is shown in dark gray, step to −40 mV is shown in black, and steps to −20 mV from −40 mV at varying intervals are shown in light gray. (b) Individual current recordings from synaptically coupled RBC-AII pairs showing typical AII EPSCs in response to V_{RBC} voltage steps described in panel a. Shades of current traces correspond to colors shown above. (c) Average integrated current (± SD; n = 7 cells) measured over the transient component of the response, plotted as a percentage of charge transfer in response to the −70 to −20 mV step. Open symbols show the arithmetic sum of the transient responses to the −70 to −40 and −40 to −20 mV responses. Deviation from of the −20 mV response during the shortest time interval reflects an over-subtraction of the baseline from the preceding transient response.

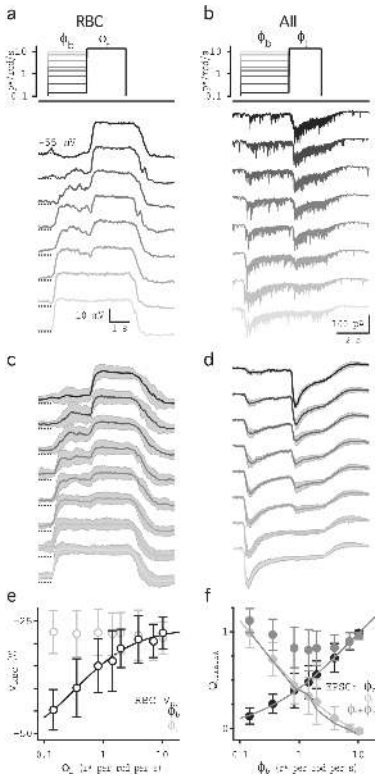

Fig. 5.

RRP occupancy encodes luminance. (a) Perforated-patch current-clamp recordings from a single RBC show voltage responses to steps in φ for full-field light stimulation. Schematic shows the light intensity of each step corresponding to the voltage traces shown below. (b) Whole-cell voltage-clamp recordings from a single AII amacrine cell in response to the same light stimulation protocol used in (a). (c) Average (± SD, gray shading) light responses in 5 RBCs. Traces were down sampled to 1kHz resolution before averaging. (d) Average (± SD, gray shading) light-evoked EPSCs in 10 AIIs. Traces were down sampled to 0.1kHz and smoothed with a 12 Hz cutoff Gaussian filter before averaging. (e) Average voltage responses (± SD; n = 5 cells) to φ_b and φ_t plotted against φ. Solid black line is the Hill equation fit to $V_{RBC}(\varphi_b)$. (f) Average integrated current (± SD; n = 10 cells) measured over the transient component of the response to φ_b (black) and φ_t (light gray), plotted against φ_t Solid black and light gray lines represent the Hill equation fits to $Q_t(\varphi_b)$ and $Q_t(\varphi_t)$, respectively. Dark gray symbols indicate the sum (average ± SD; n = 10 cells) of transient responses to φ_b and φ_t. Dark gray line shows the arithmetic difference between $V_{RBC}(\varphi_t)$ and $V_{RBC}(\varphi_b)$.

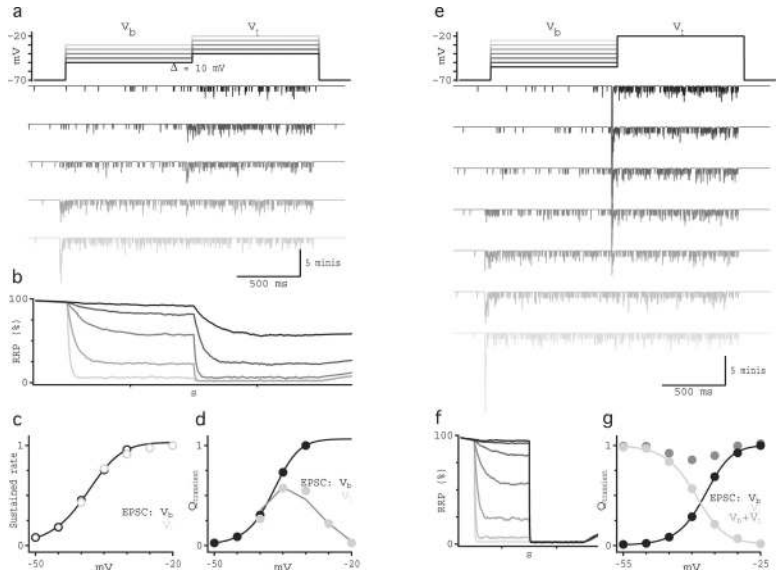

Fig. 6.

Synaptic simulations suggest that a homogeneous RRP is sufficient to encode a measure of contrast and luminance. (a) Schematic of the voltage protocol used in the paired recordings in figure 2. Simulated traces below show the "current" output from the model (see methods) for a single trial with an RRP size of 55 vesicles. (b) As in (a), but with the voltage protocol used in the paired recordings in figure 3. (c) RRP occupancy vs. time for the simulations in (a). (d) The sustained rate of simulated vesicle release measured in (a) over the last 0.5 s of the step to V_b (black) and V_t (gray) vs. V_{RBC}. Solid line shows the Hill equation fit to the simulated data points. (e) Integral of the "current" during the transient component of the responses in (a) to V_b (black) and V_t (light gray). Dark gray line shows the subtraction between the rate(V_t) and rate(V_b). Solid black line shows the Hill equation fit to the measurements of Q(V_b). (f) RRP occupancy vs. time for the simulations in (b). (g) Integral of the "current" during the transient component of the responses in (b) to V_b (black) and V_t (light gray) vs. simulated V_{RBC}. Solid lines shows the Hill equation fit to the measurements for Q(V_b) (black) and Q(V_t) (light gray). Dark gray symbols show the sum of the transient responses to V_b and V_t. The data in panels c–g reflect an average of 40 trials for an RRP size of 55 vesicles.

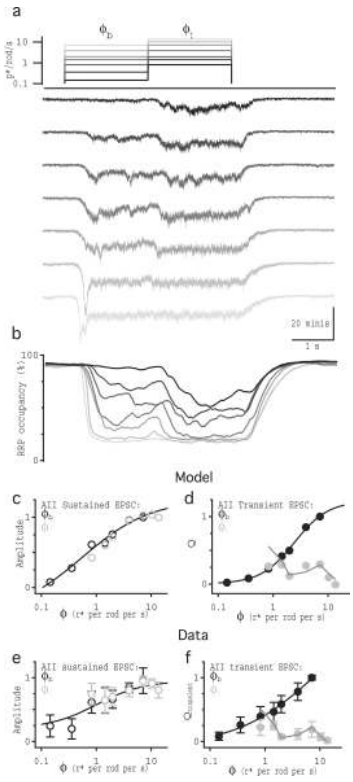

Fig. 7.

The synaptic release model can encode luminance and compute contrast from light-evoked RBC waveforms (a) Schematic of the light intensity steps used in the light stimulation protocol used in figure 1. Each RBC voltage response measured in the experiment in figure 1 was used as the voltage input to the model with an RRP size of 2400, and the average of these five modeled "current" outputs are shown. (b) Average RRP occupancy from the five light-evoked V_{RBC} runs. (c) Amplitude of simulated EPSCs measured over the last 0.1 s of φ_b (black) and φ_t (light gray) vs. f. Solid line is the Hill equation fit to the data. (d) Integrated current measured over the transient component of the response to φ_b (black) and φ_t (light gray), vs. φ. Dark gray line shows the scaled contrast step size between φ_b and φ_t, vs. φ_t. Solid black lines are the Hill equation fit to the data. (e) and (f) reproduce panels from figure 1c and h for comparison between experimental and simulation results.